

Investigation of NO₂ Pollutions on Board of Research Aircraft (Some Results of QUANTIFY and POLARCAT Field Campaigns)

N. Sitnikov^{*}, V. Sitnikova, A. Ulanovskiy, A. Lukyanov
Central Aerological Observatory, Russia

H. Schlager, A. Roiger, M. Scheiber, M. Lichtenstern and P. Stock
Deutsches Zentrum für Luft- und Raumfahrt, Oberpfaffenhofen, Germany

F. Ravegnani
Istituto di Scienze dell' Atmosfera e del Clima, Bologna, I-40129 Italy

Keywords: Air Pollutions, Ship Emissions, Nitrogen Oxides

ABSTRACT: The results of investigation of NO₂ pollutions on board of research aircraft Falcon (DLR, Germany) are presented. The measurements have been carried out by chemiluminescent nitrogen dioxide analyzer developed in Central Aerological Observatory (Russia). The data of NO₂ distribution have been obtained during QUANTIFY (West Europe, July 2007) and POLARCAT (Greenland, July 2008) field campaigns. NO₂ measurements over Greenland during POLARCAT field campaign have been carried out using ACCENT support. Different sources of nitrogen oxides are investigated. Some aspects of nitrogen dioxide distribution and transport are considered. Chemical transformation of nitrogen oxides inside ship plumes is observed and analyzed.

1 INTRODUCTION

Aircraft measurements of NO₂ atmospheric pollutions have been carried out using chemiluminescent nitrogen dioxide analyzer developed in Central Aerological Observatory (Russia). They were performed on board of research aircraft "Falcon" (DLR, Germany) during Quantify (July 2007, Brest, France) and POLARCAT (June 2008, Greenland) field campaigns. First one was concerned to ship emission measurements in the major European ship corridor. Ship emission is very important component of anthropogenic environmental pollution which gives considerable impact of greenhouse gases, aerosols and another substances to atmosphere. There are some publications concerning experimental investigations and modeling studies of ship emission (Corbett and Fischbeck, 1997, Schlager et al. 2006, Petzold et.al. 2006). Chemical transport models parametrization needs detail information about chemical and photochemical reactions in atmosphere of polluted regions including exhaust plumes. Simultaneous measurements of different gas species permit to investigate chemical and photochemical processes in atmosphere including the processes inside individual exhaust plume. Specially developed chemiluminescent nitrogen dioxide analyzer has a high time (~0.2 sec) and space (~20m) resolution, which is important to make correct measurements of NO₂ distribution in small size ship emission plumes. Another experience of using this instrument on board of research aircraft "Falcon" was in POLARCAT field campaign in June 2008 in Greenland. The objectives of the campaign are to investigate the impact of urban and forest fire emissions in the Arctic troposphere, mechanisms of fire plume spreading (dispersion, mixing), chemical and photochemical transformations in the fire plumes, and impact of forest fire emission transported by pyroconvection into the lower stratosphere.

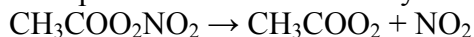
^{*} *Corresponding author:* Nikolay Sitnikov, Central Aerological Observatory (CAO), Dolgoprudny, Moscow region, Russia. Email: sitnikov@caomsk.mipt.ru

2 METHOD AND INSTRUMENT

The instrument is based on chemiluminescent principle (Kinrade, 1991) that is interaction of NO₂ with luminol solution leads to light radiation in visible spectral range. The intensity of the light depends on the nitrogen dioxide concentration. This method is very fast and very sensitive to NO₂ but it has some interference in atmosphere. The highest interference is sensitivity to peroxyacetyl nitrate (PAN), which is about 25% of NO₂ sensitivity. For correct NO₂ measurements it must be taken into account. Another interference is the sensitivity to ozone. It is not so high (less than 0.5% of NO₂ sensitivity) and it can be excluded by additional O₃ measurements or using special ozone scrubber. Special design of the instrument permits to take into account PAN influence. Ozone influence is excluded using “Falcon” ozone data.

The block diagram of the instrument is shown in Fig.1. Main sensor (Sitnikov et.al 2005) consists of liquid pump with special valve, reaction chamber and photoelectric multiplier (Fig.1a). Liquid pump for circulating the liquid is a syringe filled with a chemiluminescent solution. Its plunger is slowly displaced by a reduction motor. In order to exclude the possibility of the chemiluminescent solution boiling at low pressures and the appearance of flow-velocity instabilities, valve is connected to the pump outlet. This valve obstructs the chemiluminescent solution flow; as a result, the pressure inside the syringe during the movement of the plunger always exceeds atmospheric pressure. A nipple manufactured from such neutral materials as silicone, teflon, polyethylene, etc., can serve as a valve. This design of the pump completely excludes the possibility of bubble formation and ensures a constant liquid flow at external pressures of 1 to 1000 mbar. The consumption of the chemiluminescent solution is determined only by the velocity of the plunger's motion and amounts to 2.5 ml/h; i.e., 10 ml of the solution sustains the operation of the instrument for 4 hours that is for usual duration of “Falcon” flight. The pump supplies the solution into the reaction chamber and onto a porous substrate. The exhausted solution drains off into a vessel positioned below the reaction chamber.

The instrument includes two channels (main and auxiliary) with two chemiluminescent sensors (Fig.1b). One of them (auxiliary channel) has PAN-NO₂ converter (thermolytic cell) which is heated up to 200-250°C. Thermolytic destruction of PAN provides increasing of NO₂ concentration:



This results in signal increasing in auxiliary channel because of different sensitivity to NO₂ and PAN. Simultaneous measurements in two channels permit to take into account the influence of PAN and increase the accuracy of NO₂ measurements. Ozone influence is corrected using the data of “Falcon” ozone measurements. Calibration of the instrument was performed in CAO and DLR. Fig.1c illustrates the process of measurements with correction taking into account PAN influence. Usually this correction was not high.

Air flow through the main and auxiliary channels (about 2 l/min) is provided by air pump with constant volume flow rate. The instrument is regulated by compact electronic block. It can operate in automatic regime. The data of measurements is recorded to internal flash memory. The instrument has RS232 interface for connection with computer or telemetry system.

Technical characteristics of the instrument:

The range of NO ₂ measurements	0.05 – 100 ppbv;
Time resolution	0.2 s
Weight	5 kg;
Power	50 W.

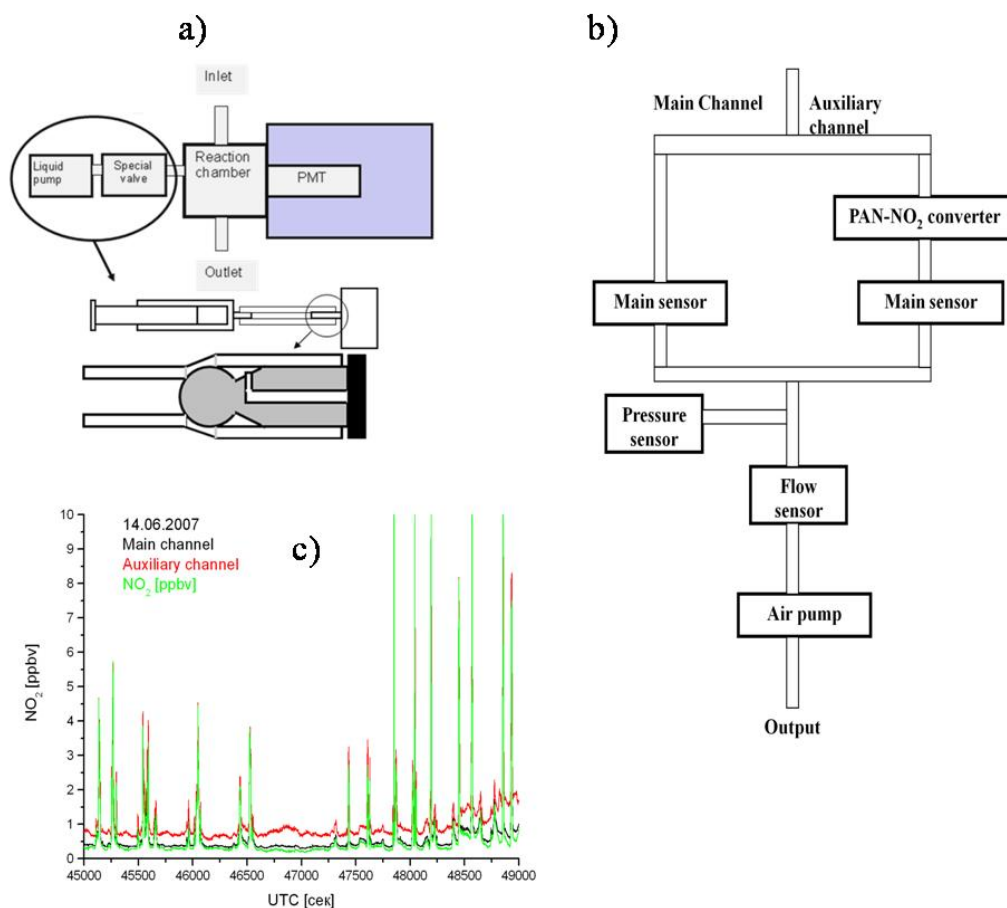


Fig.1. Block diagram of the main chemiluminescent sensor (a) and chemiluminescent nitrogen dioxide analyzer (b) and time series of signals (in terms of NO₂ concentration) in main channel (black), auxiliary channel (red) and NO₂ concentration corrected taking into account PAN influence (green).

3 RESULTS AND DISCUSSIONS

Eight scientific flights were fulfilled in June 2007 during Quantify project field campaign by scientific aircraft Falcon in different routes. The altitudes changed from several hundred meters to several kilometers, the duration of flights was 3 – 3.5 hours. The measurements were made above the Atlantic Ocean as in non polluted areas as in sea transport corridor, the most polluted regions of Europe. Distribution of some atmospheric species such as nitrogen oxides, CO, CO₂, aerosols and others has been measured. NO₂ measurements were fulfilled by chemiluminescent nitrogen dioxide analyzer described above. Time response of the instrument was 0.2 sec. As the aircraft velocity was 100 m/sec, space resolution of NO₂ concentration measurements was about 20 m. Some results of nitrogen dioxide measurements are represented in Fig. 2-4.

The flight on 14th of June, 2007 was from Brest (France) to western coast of England as demonstrated in Fig.2. Different chemical components concentrations were measured in a dedicated exhaust plume of a large container ship (Atlantic Conveyor flight). During the flight the aircraft crossed the exhaust plume many times at different distances from the ship. Several trace species concentrations were measured for different life times of the exhaust plum (from 1 minute to several hours). Fig.2 represents NO and NO₂ concentrations measurements for the part of flight on the 14th of June, 2007. As the measurements were strictly synchronized we can determine dependence of NO₂ / NO_x ratio from the life time of the exhaust plum. The results of the calculation are represented in Fig.2b. As figure shows initial NO₂/NO_x ratio is very low (about 0.1). Then it increased up to 0.6 – 0.7 during some minutes. This increasing is connected with fast chemical reaction of NO with ozone, and after that variation of NO₂/NO_x ratio was not high during some hours.

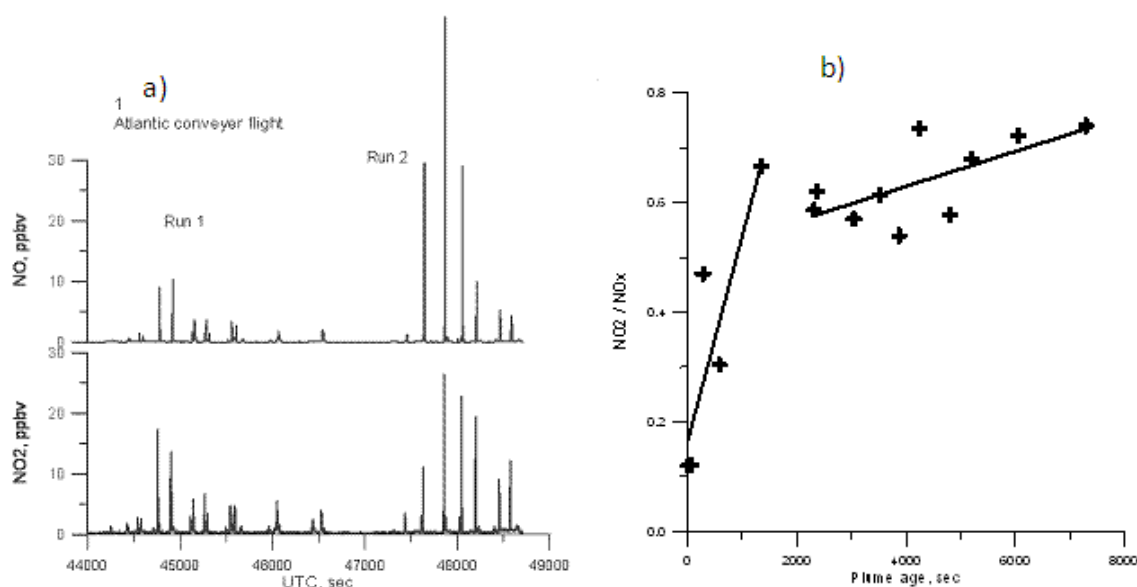


Fig.2. Time series of simultaneous NO and NO₂ measurements during Atlantic conveyor flight July 14, 2007 (a) and the ratio NO₂/NO_x versus plume age calculated from this data (b).

On the 17th of June there were two flights along English Channel from Brest to Bremen (Fig.3a) and back to Brest (Fig.3b). The first flight from Brest to Bremen was started early in the morning. The second flight from Bremen to Brest was several hours later. NO₂/NO_x ratios were calculated from the results of measurements in peaks of exhaust plumes of different ships. Fig.3c demonstrates the dependence of NO₂/NO_x ratio from the day time for both flights on the 17th of June. Decrease of the ratio with time most likely associated with dependence of photochemical reactions rate from the Sun radiation intensity. Average NO₂/NO_x ratio was 0.85 for the first flight and 0.64 for the second one. However NO₂/NO_x ratio of every flight has spreading in its values. This spreading is probably connected with different plume ages or different weather conditions in different points of the route.

The measurements demonstrated that NO₂ distribution in a major ship corridor near Western coast of Europe highly inhomogeneous. Background NO₂ concentrations were less than 0.5 ppbv. Local maximums which caused by ship emission were found about several tens of ppbv, sometimes more than 100 ppbv. Such concentrations were measured at altitudes less than 500 meters. At altitudes above 500 meters as a rule background NO₂ concentrations were measured.

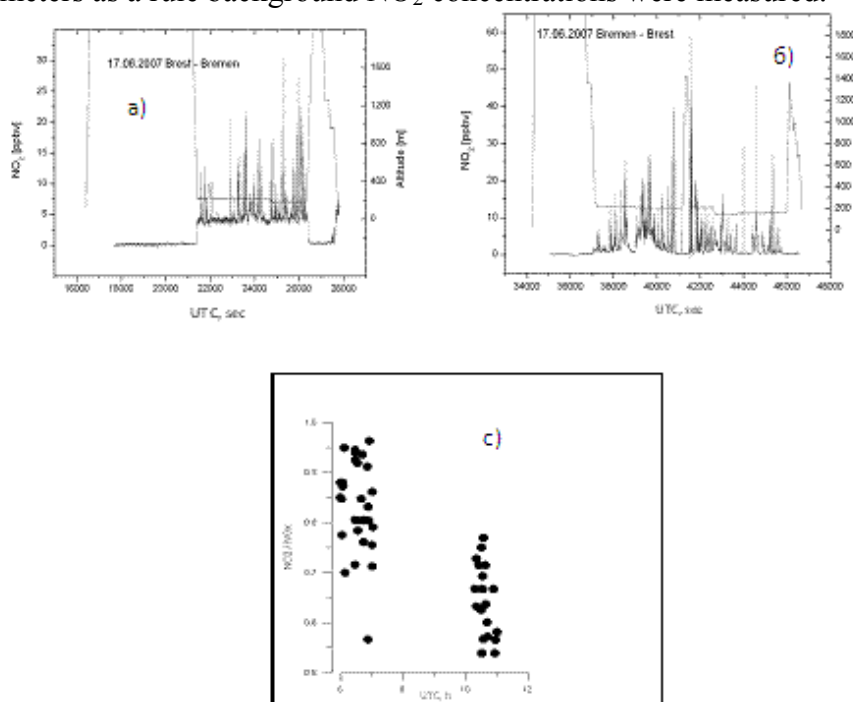


Fig.3. Time series of NO₂ concentration in ship corridor which is measured 17.06.2007 during the flights Brest-Bremen (a) and Bremen-Brest (b) and NO₂/NO_x ratio versus day time (c) calculated from NO₂ and NO local maxima.

Another experience of using nitrogen dioxide analyzer on board of research aircraft was during POLARCAT field campaign in June 2008. The campaign is based in Kangerlussuaq (Greenland). There were some flights with different routes to make measurements of atmospheric species from urban and forest fire emissions of North America and Siberia. In most of flights the measurements show very low NO₂ concentrations. There were nearly or lower the detection limit of the instrument (some tens of pptv). Maximal NO₂ concentration (about 200 pptv) has been observed during the flight of July 10, 2008. (Fig.4b) The flight was performed over the Greenland in North direction (Fig.4a) mainly in stratosphere. Fig.4c shows 10 days backward trajectories from initial points with increased NO₂ concentration. Considered air masses with increased NO₂ concentration have different origin. As trajectory analysis shows the origin of air masses with increased (in comparison with phone concentrations) NO₂ concentration is not connected with lower troposphere.

Then according to completed measurements, the considerable increasing of NO₂ concentration in Arctic connected with forest fire is not observed during POLARCT field campaign.

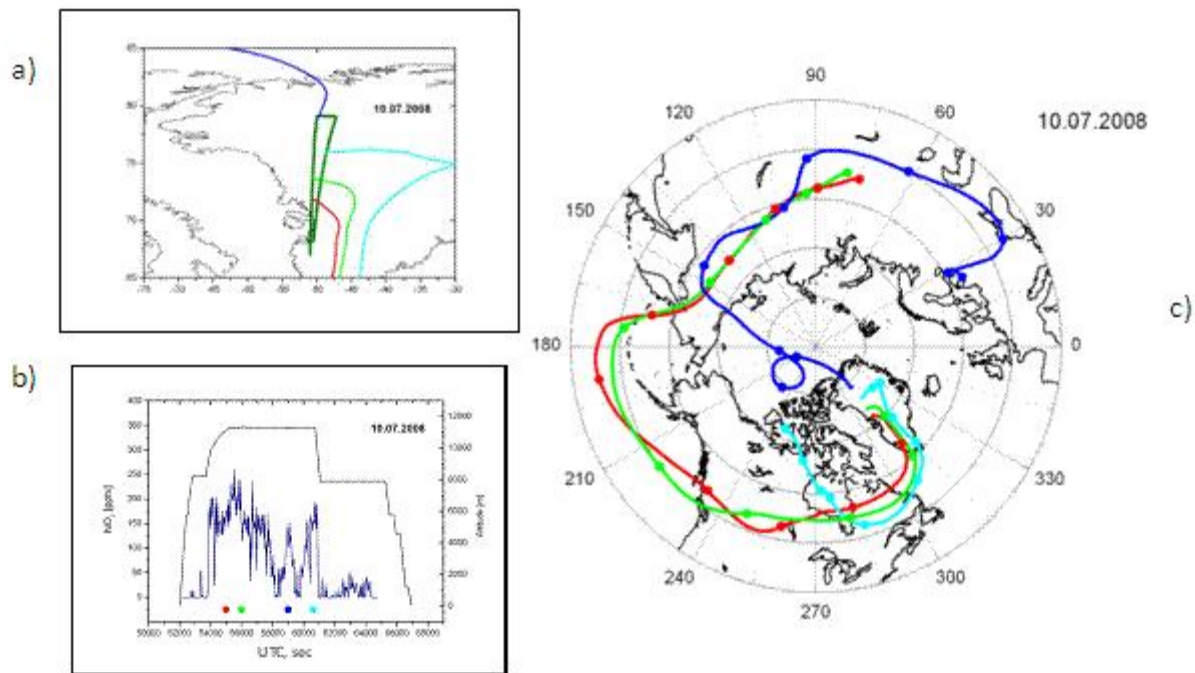


Fig.4. The route of research aircraft “Falcon” flight 10.07.2008 (a), time series of NO₂ measurements during this flight (b), 10 days backward trajectories of air masses plotted from initial points with maximal NO₂ concentration (c).

4 CONCLUSIONS

In the frame of European project QUANTIFY in Central Aerological Observatory Chemiluminescent Nitrogen Dioxide Analyzer for research aircraft have been developed and manufactured. NO₂ measurements on board of research aircraft “Falcon” during QUANTIFY (June 2007) and POLARCAT (July 2008) field campaigns have been carried out using developed instrument. NO₂ measurements in European ship corridor during QUANTIFY field campaign showed very inhomogeneous NO₂ distribution from concentrations < 0.5 ppbv up to 100 ppbv connected with ship emission. Data analysis of the of simultaneous NO and NO₂ measurements shows nitrogen oxides chemical transformation inside the individual exhaust plume.

5 ACKNOWLEDGEMENTS

Many thanks to “Falcon” team for the help during field campaigns. NO₂ measurements in POLARCAT field campaign have been carried out due to ACCENT support.

REFERENCES

- Corbett, J.J. and P.S. Fischbeck, 1997: Emissions from ships, *Science* 248, 3723-3731.
- Kinrade John D. Patent 5.015.590 US. // Scintrex Limited (Concord, CA), 1991.
- Petzold A., B. Weinzerl, M. Fiebig, Lichtenshtern M., P. Lauer, C. Gurk, K.Franke, E. Weingartner, 2006: Particle emissions from ship engines: emission properties and transformation in the marine boundary layer, *Proceedings of the TAC-Conference, June 26-29, 2006, 78-82, Oxford, UK.*
- Schlager H., R. Baumann, M. Lichtenstern, A. Petzold, F.n Arnold, M. Speidel, C. Gurk, H. Fisher, 2006: Aircraft-based trace gas measurements in a primary European ship corridor, *Proceedings of the TAC-Conference, June 26-29, 2006, 83-88, Oxford, UK.*
- Sitnikov N.M., A.O. Sokolov, F. Ravegnani, V.A. Yushkov and A.E. Ulanovskiy: A chemiluminescent balloon type nitrogen dioxide meter for tropospheric and stratospheric investigation (NaDA), *Instruments and Experimental Techniques Vol. 48, No. 3, 2005, pp. 400-405.*

High resolution simulations of aircraft condensation trails: Contrails Evolution and Diffusion

Sarrat, C.* , R. Paugam¹, R. Paoli, D. Cariolle, L. Nybelen

*European Centre for Research and Advanced Training in Scientific Computation, CERFACS/CNRS,
Toulouse, France*

¹ *Now at Department of Geography, King's College London, London, UK*

Keywords: Contrails, Diffusion, transition contrail-to-cirrus

ABSTRACT: This study describes a high-resolution numerical simulation of the evolution of an aircraft condensation trail (contrail) and its transition into a contrail-cirrus. The results show the extension of the contrail over 3200m width during a few hours. In particular, we show that the vertically integrated optical thickness is maintained in the core of the contrail during four hours.

1 INTRODUCTION

Contrails and aircraft-induced cirrus clouds are the most uncertain contributors to the Earth radiative forcing, among all aircraft emissions, according to the latest estimations by Sausen, et al. (2005).

If the conditions for contrails formation and persistence are now well accepted ($RH_w > 100\%$ and $RH_i > 100\%$, where RH_w , RH_i are the ambient relative humidity with respect to water and ice, respectively), the details of the transformation of contrails, and in particular the critical phase of transition from linearly shaped contrails to widely spread cirrus, are still unclear.

One of the reasons for this uncertainty is the very complex dynamical and physical interactions that occur in aircraft wakes.

As proposed by Gerz et al. (1998), these interactions can be represented as four successive regimes. The two first regimes, (respectively the jet and vortex regimes) last a few minutes after emissions, and correspond to the interaction between the engines exhaust and the vortices generated by the wings, and the formation of the primary and secondary wakes. During the following minutes, the vortices breakup and generate turbulence (dissipation regime). During the last diffusion regime, the contrail evolution is controlled by the atmospheric background conditions. The aim of the present study is to carry out a direct dynamical large-eddy simulation of the diffusion regime where contrail-to-cirrus transition takes place.

2 MODEL PRESENTATION

The contrails simulations are performed with Meso-NH, a meteorological, non-hydrostatic meso-scale model (Lafore et al, 1998, see also <http://mesonh.aero.obs-mip.fr/mesonh/>).

The atmospheric Meso-NH model includes the wind components (u , v , w), the Turbulent Kinetic Energy (TKE) and the potential temperature (θ) as prognostic variables, whereas a dedicated microphysical scheme specific for contrails is implemented to simulate the ice crystal variable together with the condensation, evaporation and sedimentation process (see Paugam et al., 2009 for details).

The microphysical scheme adds three variables to the model: the number density of ice particles n_i , the mass density of the ice phase ρ_i and the water vapour density ρ_v .

We assume locally mono-dispersive and spherical ice particles within a computational cell which yield to the relation between ρ_i and the mean particle radius r_i :

* *Corresponding author:* Sarrat, CERFACS, 42 avenue Coriolis, 31057 Toulouse. Email: sarrat@cerfacs.fr

$$\rho_i = \frac{4}{3} \pi r_i^3 \rho_{ice} n_i$$

We present here the simulation from 35 minutes to few hours after the aircraft release.

The model is initialized at 2120s using the outputs of Meso-NH simulations from Paugam et al. (2009).

A specific model configuration is used in order to maintain a synthetic turbulence that is representative of the background atmospheric turbulence at the tropopause level.

This is based on the 2 domain-nesting functionality of Meso-NH: in the father model, an unstable stratified shear flow is used to generate turbulent fluctuations of velocity and potential temperature.

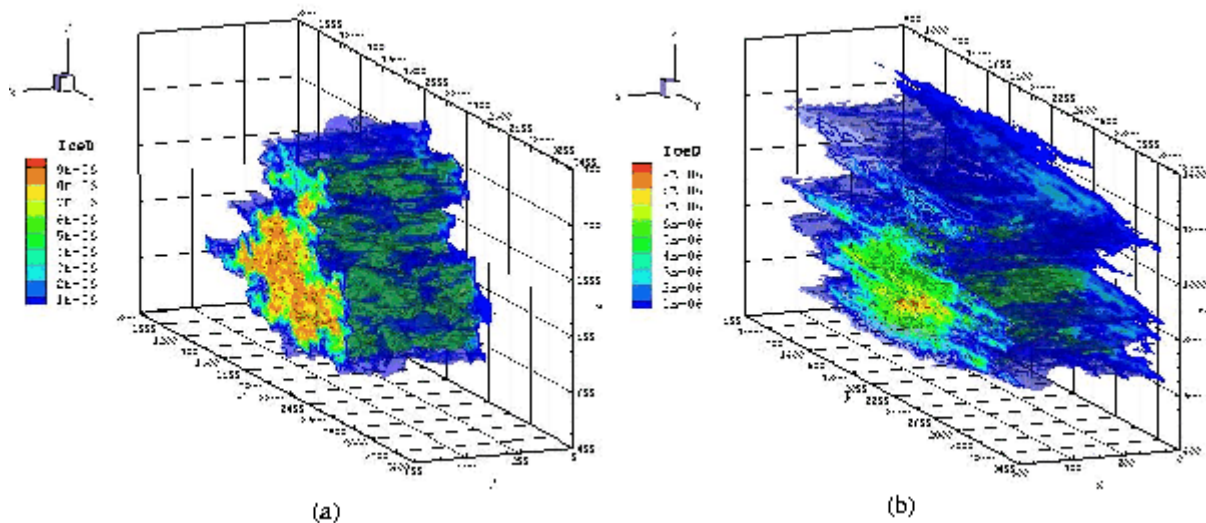
These fluctuations are afterwards injected in the son model in which the contrail is simulated.

The dimensions of both domains are: $L_x = 500$ m, $L_y = 4000$ m and $L_z = 1500$ m, with the same resolution in the 3 directions ($\Delta x = \Delta y = \Delta z = 10$ m).

8 MODELING RESULTS

The Meso-NH simulations presented here correspond to the diffusion regime, i.e. the contrail-to-cirrus transition. Starting from 35 minutes after emission, the simulation lasts almost four hours.

Figure 1 presents the simulated ice density in a three dimensional figure, where the x axis is along the direction of the flight. Only a contrail fraction of 500 m is simulated as represented in Figure 1. At $t=2120$ s (Figure 1a), the contrail core contains a large amount of ice, while the primary and secondary wakes are still visible. A few hours later, (at $t=10120$ s, Fig. 1b), the horizontal extension of the contrail perpendicularly to the aircraft trajectory increases from 1300 m to 3200 m. At this stage



of the diffusion regime, the primary and secondary wakes are almost merged.

Figure 1: Three-dimensional view of the contrail. The x-axis indicates the flight direction. The colored iso-surfaces represent the ice density: (a) at $t=2320$ s and (b) at $t=10120$ s.

The mean particle radius is displayed in Figures 2a and b. The larger particles are located at the top and the bottom of the contrail, where their number is lower: the ice particles grow faster because the water vapour available for condensation in the supersaturated ambient air is higher. On the other hand, in the contrail core, where most of the particles were trapped by the vortex, the growth is damped because the same amount of background water vapour has to be shared among more particles.

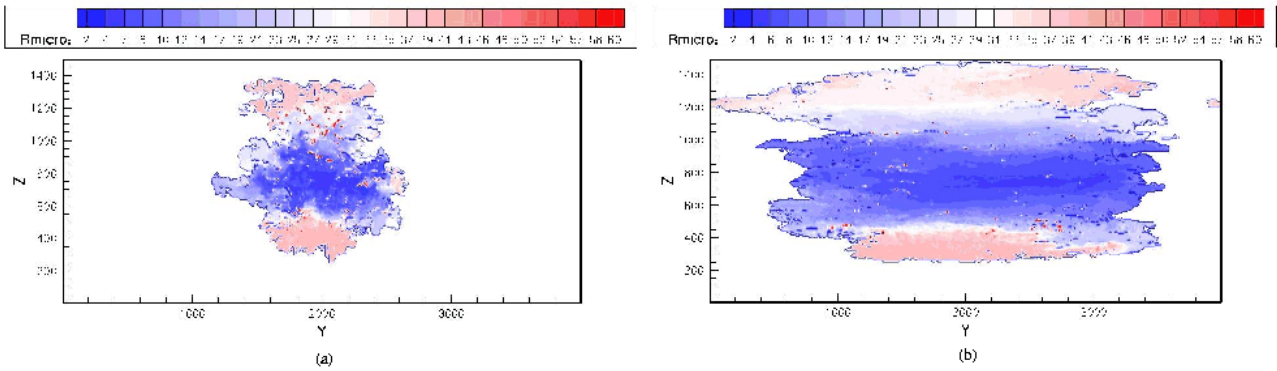


Figure 2: Vertical cross section at $x=250\text{m}$ of the ice particle mean radius: (a) at $t=2320\text{s}$ and (b) at $t=10120\text{s}$.

As shown in the Fig. 3, the vertically integrated optical thickness is maximum in the middle of the contrail, where the number of particles is the highest and rapidly falls next to the edge of the cloud. The optical depth remains rather high during the simulation, decreasing from 0.95 to 0.55, through the four hours of simulation in agreement the study of Jensen et al. (1998). In fact, even if the ice density decreases because of contrail spreading, the ice particles radius grows in such a way that the optical depth is maintained.

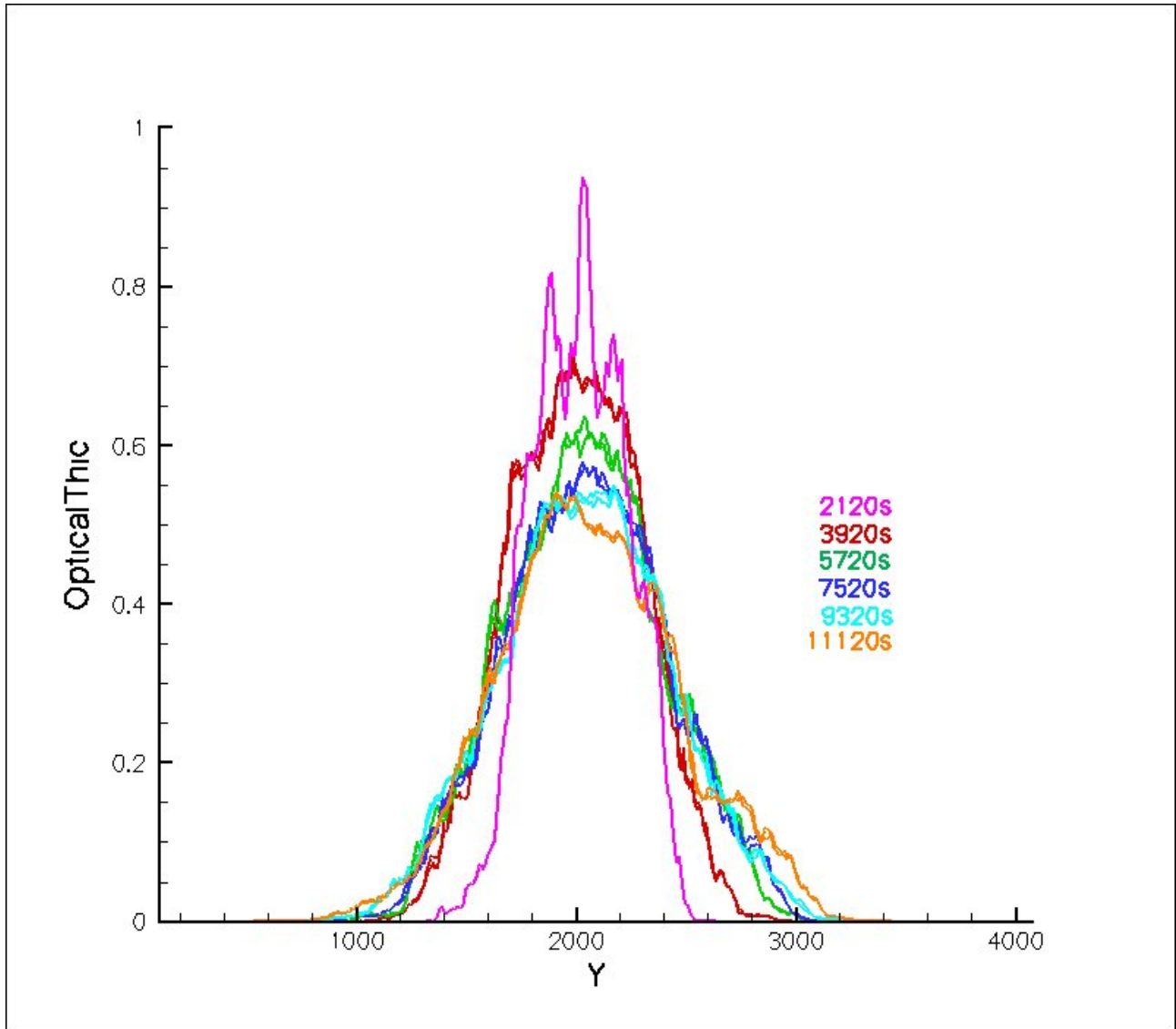


Figure 3: Contrail’s optical thickness as a function of the horizontal axis, perpendicular to the flight direction. The optical thickness is integrated over the vertical direction. Colours identify time.

4 CONCLUSION

We use a three-dimensional non-hydrostatic meteorological model to describe the evolution of a contrail in the diffusion regime.

Four hours of the transition contrail to cirrus are simulated. The results show the horizontal contrail spreading over 3200 m width, while the vertical extent remains limited.

At this stage of the dissipation regime, the primary and secondary wakes are not separated any more.

The model is able to maintain a high optical depth because of the simultaneous decrease of ice density and increase of ice mean radius in the growing contrail, as the result of condensation of ambient water vapour.

The mean radius at the top and bottom of the cloud reaches 50 to 55 μm , allowing sedimentation. In this study, we don't activate the sedimentation parameterization, but we expect that the particles radius is large enough to have a fall velocity not negligible any more. As a consequence, the sedimentation impact of the vertical distribution will be addressed in a follow-up study.

5 ACKNOWLEDGEMENTS:

The authors would like to thank the French National Computing Centre for Higher Education (CINES) for the attribution of computational hours, used for this study.

REFERENCES

- Gerz, T., Dürbeck, T., and Konopka, P., 1998: Transport and effective diffusion of aircraft emissions, *J. Geophys. Res.*, 103, 25 905–25 914.
- Jensen, E., Ackerman, A., Stevens, D., Toon, O., and Minnis, P., 1998: Spreading and growth of contrails in a sheared environment, *J. Geophys. Res.*, 103, 31,557–31,567.
- Lafore, J., Stein, J., Bougeault, P., Ducrocq, V., Duron, J., Fischer, C., Hérelil, P., Mascart, P., Masson, V., Pinty, J.-P., Redelsperger, J., Richard, E., and de Arellano, J. V., 1998: The Meso-NH atmospheric simulation system. Part I: adiabatic formulation and control simulations, *Ann. Geophys.*, 16, 90–109.
- Paugam, R., Paoli, R., and Cariolle, D., 2009: Three-dimensional numerical simulations of the evolution of a contrail and its transition into a contrail-cirrus, *ACPD*, 9.
- Sausen, R., Isaksen, I., Grewe, V., Hauglustaine, D., Lee, D. S., Myhre, G., Khler, M. O., Pitari, G., Schumann, U., Stordal, F., and Zerefos, C., 2005: Aviation radiative forcing in 2000: an update on IPCC (1999), *Meteorol. Zeitschrift*, 14, 555–561.

The Effect of Ice Particles on the Tropospheric Ozone Budget via Heterogeneous Conversion processes

J. E. Williams^{*}, G.-J. van Zadelhoff and P.F.J. van Velthoven
Koninklijk Nederlands Meteorologisch Institute, De Bilt, The Netherlands.

Keywords: Cirrus, Heterogeneous Processes, Future Emissions

ABSTRACT: Cirrus particles are ubiquitous throughout the mid- to upper troposphere and provide reactive surfaces onto which trace gas species may become either attached or chemically processed, thus modifying the chemical cycles active at high altitudes. Here we introduce two simple parameterizations for the description of the micro-physical properties of ice particle fields into a global 3D Chemistry Transport Model. We subsequently investigate the influence that the reversible loss of HNO₃ from the gas phase has on the tropospheric ozone budget. In contrast to previous studies there is a modest increase in the global tropospheric ozone burden, where there are stark hemispheric differences. By applying the EU-QUANTIFY 2050 aircraft emission scenarios using fixed meteorology for 2006 we show that the influence of heterogeneous scavenging becomes less important unless the available surface area upon which scavenging can occur would increase in the future.

1 INTRODUCTION

Ice particles form readily throughout the troposphere and may grow to significant sizes depending on both the ambient temperature and the partial pressure of water vapour. Once present they introduce both perturbations to the radiation budget and reactive surfaces upon which trace gas species may become either reversibly or irreversibly attached, depending on the chemical structure of the chemical species and their characteristic affinity for the ice surface. One such trace gas species which has a high affinity for being scavenged on ice is nitric acid (HNO₃). In the upper troposphere HNO₃ acts as an abundant reservoir species for reactive nitrogen, which, once oxidised, helps determine the *in-situ* formation of tropospheric ozone (O₃). By scavenging HNO₃ out of the gas-phase, a fraction of this reactive nitrogen is essentially removed (sequestered) from the gas phase, which has the potential to lower *in-situ* O₃ formation. Laboratory studies have determined the kinetic parameters needed to describe this reversible uptake and have found that saturation of the ice surface maybe accounted for by using a parameter to describe the maximum number of reactive sites available per cm² of ice surface (Cox et al, 2005). This uptake parameter is commonly known as the Langmuir uptake co-efficient. Here we introduce parameterizations into the global Chemistry Transport Model (CTM) TM4 for the calculation of the available reactive surface area utilizing the Ice Water Content (IWC) available from ECMWF meteorological data and investigate the effects of reversible scavenging of HNO₃ out of the gas phase.

2 DESCRIPTION OF THE CTM

The version of TM4 used in this study is similar to TM4_AMMA described in Williams et al (2009) apart from the application of updated heterogeneous uptake data for (e.g.) the scavenging of HCHO into cloud droplets. The gas phase conversion of N₂O₅ into HNO₃ involving water vapour is also included in the modified CBM4 scheme using the latest recommendations (Williams and Van Noije, 2008). For the present day simulations (denoted BASE and HNO₃_UP) the emissions are taken from the RETRO database (<http://retro.enes.org>) for anthropogenic and biogenic emissions and the GFEDv2 database (van der Werf et al, 2006) for biomass burning emissions. An injection

^{*} *Corresponding author:* Jason E. Williams, Koninklijk Nederlands Meteorologisch Institute, Wilhelminalaan 10, 3732GK De Bilt, The Netherlands. Email: williams@knmi.nl

height of 2km is used in the tropics (20°N-20°S), which is typical of the injection heights seen in recent measurements (Labonne et al, 2007). Moreover, a daily cycle is imposed on the biomass burning cycle, which peaks at 2pm local time as has been determined by analysing satellite data with staggered overpass times (Boersma et al (2008)) and geostationary platforms (Roberts et al, 2009). For the future simulations (denoted 2050 and 2050_HNO3_UP) aircraft emissions for the year 2050 are applied as taken from the QUANTIFY emission database. The model uses a vertical resolution of 34 layers and a horizontal resolution of 3° x 2°, where ECMWF meteorological data is applied using an update frequency of 6 hours. A spin-up period of 6 months was used for each individual simulation.

3 RESULTS

3.1 *The zonal distribution of ice particle*

For the description of ice particles we introduce the parameterization of Heymsfield and McFarquar (1996) for the derivation of the Surface Area Density (SAD), and we use the resulting cross-sectional area (A_c) in the parameterization of Fu (1996) for the calculation the effective radii (R_{eff}). Both parameterizations use the ECMWF IWC for the derivation of the respective micro-physical properties of the ice particles. A scaling ratio of 10 was used to convert A_c into SAD as suggested by Schmitt and Heymsfield (2005), which constitutes a correction for randomly shaped particles rather than spherical particles. This is higher than the values of 2-4, which are more representative of spherical particles, used in previous CTM studies (Lawrence and Crutzen, 1998; von Kuhlmann and Lawrence, 2005). Both parameterizations have been validated against a host of different in-situ measurements (e.g. Heymsfield, 2003). Figures 1a and b show the resulting zonal distribution of both the R_{eff} and SAD values for seasons DJF and JJA, respectively. The largest R_{eff} values occur in the upper troposphere (UT) in the tropics and the lower troposphere at the poles, where there is a zonal shift between the seasons. For the SAD the highest values tend to occur in the lower troposphere above 65° latitude, as determined by the frequency at which particles occur throughout the season. Analysing daily fields reveals that values of R_{eff} ranging between 50-100µm can occur (not shown), although such sizes do not show up in the seasonal means. Depending on the lifetime of the ice particles, gravitational settling can occur for the larger particles, which will re-distribute any scavenged trace species to lower altitudes.

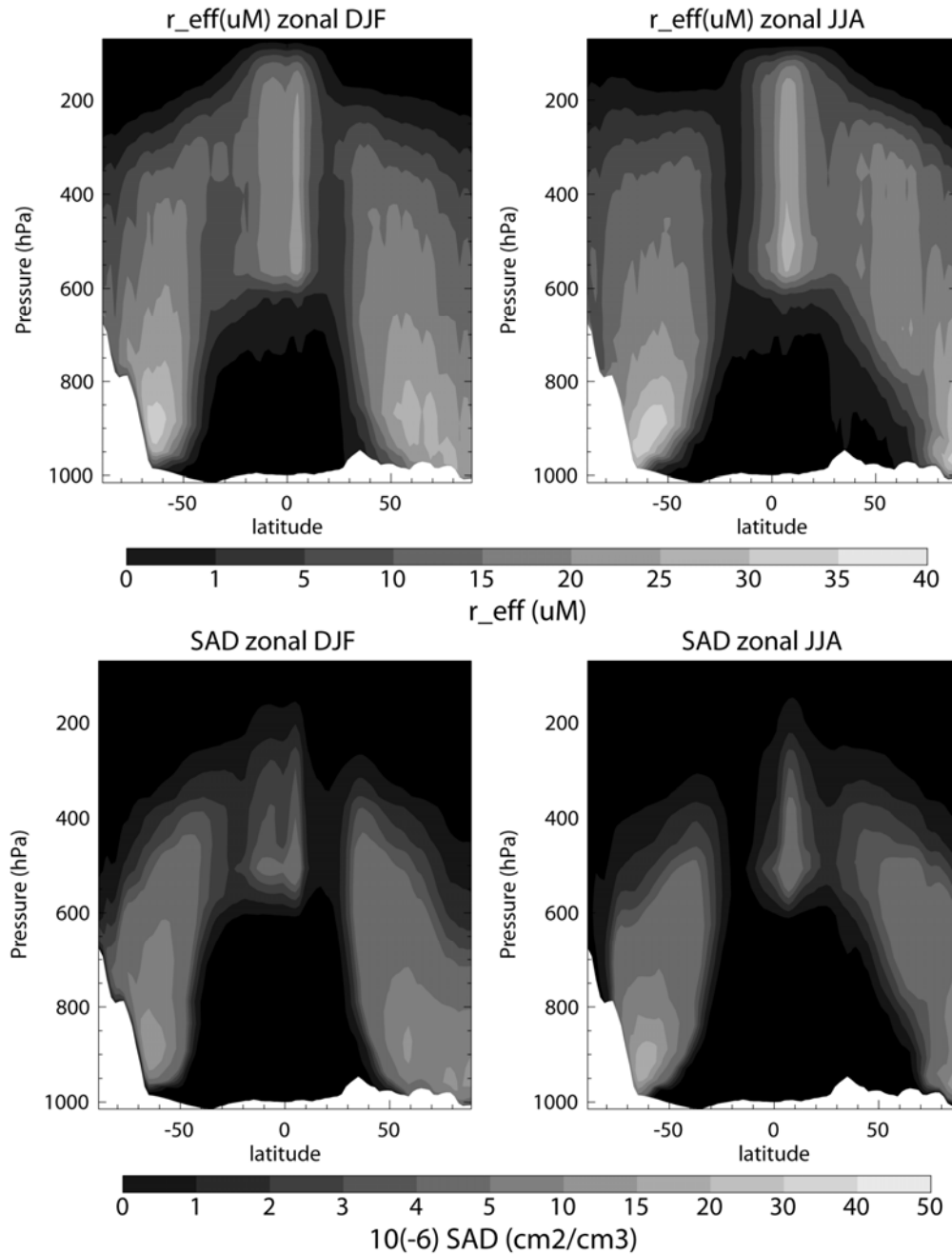


Figure 1: The zonal distribution of (top) R_{eff} and (bottom) SAD for seasons DJF and JJA when applying the chosen parameterizations for calculating the microphysical properties of ice fields online in TM4.

3.2 The effect of uptake of HNO_3 on ice surfaces for present day emissions

The uptake of HNO_3 on ice has been included in TM4 according to the latest recommendations given on the IUPAC website for chemical reaction data (www.iupac-kinetic.ch.cam.ac.uk), where the equilibrium rate is converted into a first-order absorption and desorption rate using the available SAD. It should be noted that trapping of HNO_3 by growing ice surfaces at low temperatures ($<210^\circ\text{K}$) as recently proposed by Kärcher et al (2009) is not included. Figure 2 shows the zonally integrated annual differences introduced for O_3 , NO_x , HO_x and the predominant nitrogen containing reservoir species. For the UT there are decreases in $[\text{HNO}_3]$ of $\sim 10\%$, with corresponding perturbations in $[\text{O}_3]$ of $\pm 2\%$. The differences in the lower troposphere are more moderate due to the higher temperatures which limit the available SAD. There is a clear difference in the simulated changes between the hemispheres as a result of higher $[\text{HNO}_3]$ (and $[\text{NO}_x]$) in the NH UT that are due to aircraft emissions. This uptake and subsequent release of HNO_3 causes an increase in $[\text{NO}_x]$ of between 2-5%, subsequently enhancing in-situ O_3 formation in the NH by a few percent. This is in contrast to previous studies, where decreases of between 40-60% have been simulated using NCEP meteorological data (von Kuhlmann and Lawrence, 2005). These authors did not provide in-

formation regarding the distribution of the available SAD, and no limit was placed on the number of reactive sites on the ice surface which can be occupied (*i.e.* saturation is ignored). Also a different uptake co-efficient was applied. In essence, the SAD values calculated here online in TM4 are low (20-50 $\mu\text{m}/\text{cm}^2$) compared to the range of values typically captured by in-situ measurements (20-500 $\mu\text{m}/\text{cm}^2$; Popp et al, 2004). This limits the amount of HNO_3 which can be scavenged out of the gas phase, where the low SAD is a result of the relatively large resolution adopted in the model and the ECMWF meteorological dataset (typically 1km height in the UT). This could potentially be improved upon by introducing parameterizations of sub-grid processes (e.g.) for a more accurate description of aircraft contrails (which are currently ignored). Additional sensitivity tests including gravitational settling of large particles result in differences in NO_x of $\pm 1\%$ (not shown), due to the low fraction of HNO_3 removed from the gas phase. Inclusion of a fraction of irreversible loss ('Burial'), as proposed by Kärcher et al (2009), would enhance the effects presented here by providing a NO_x sink at high altitudes. Moreover, conversion of the NO_3 radical and irreversible loss of OH on the surface of ice particles were also tested and found to have relatively small effects on the composition of the UT.

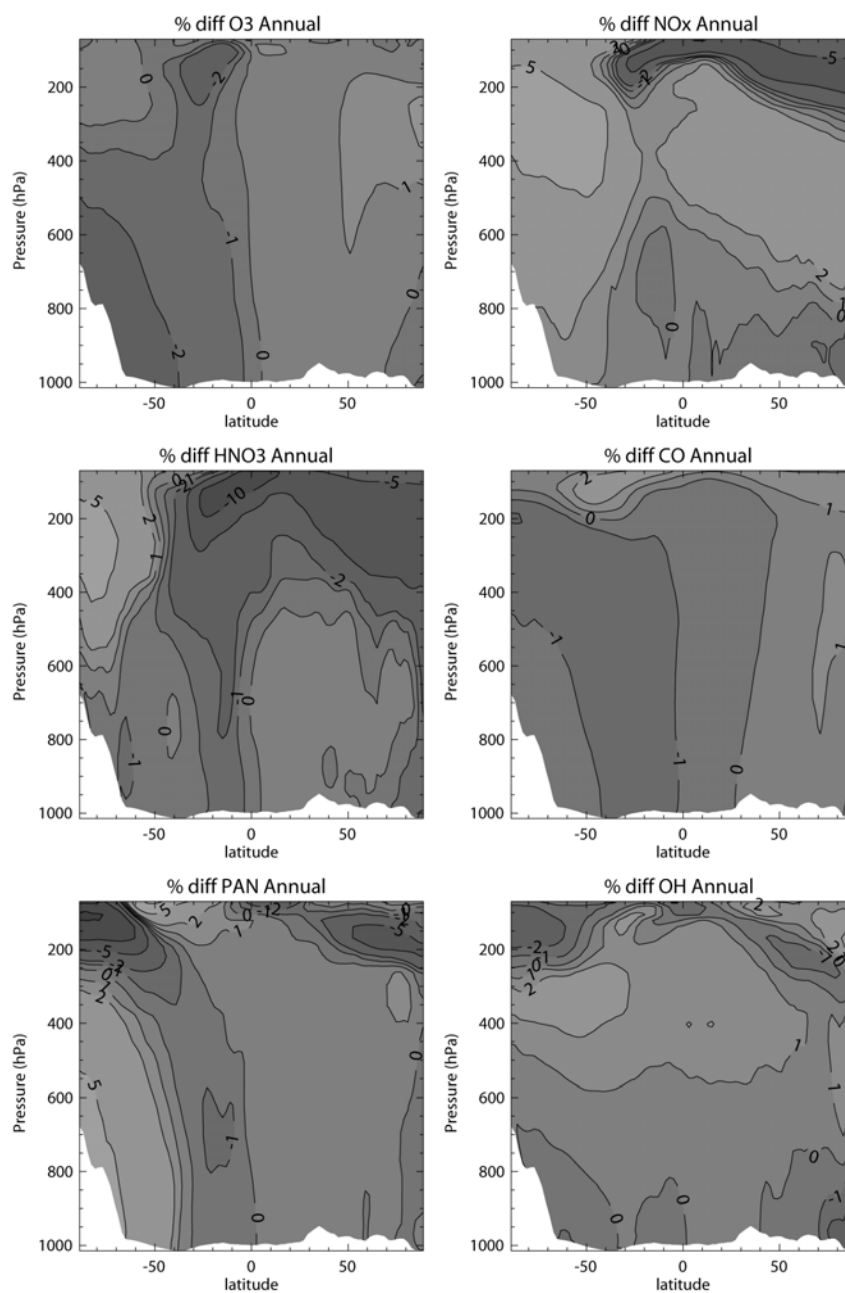


Figure 2: The zonally integrated annual differences in (a) O_3 , (b) NO_x , (c) HNO_3 , (d) CO, (e) PAN and (f) OH as a result of introducing heterogeneous uptake of HNO_3 on cirrus particles.

3.3 The effect of future aircraft emissions for the year 2050

The 2050 A1 future aircraft emissions as taken from the QUANTIFY project (www.pa.op.dlr.de/quantify) increase the annual global nitrogen budget by ~ 4.5 Tg N, where the additional NO_x is predominantly injected between 200–600 hPa in the NH. Here we apply the meteorology for 2006 in order to differentiate the influence of increasing the aircraft emissions towards the future estimates from possible meteorological differences in future years. Figure 3 shows the resulting increases in the zonally integrated annual means for O_3 , NO_x and HNO_3 . For $[\text{NO}_x]$ increases of $>200\%$ occur between 200–400 hPa, which increases the tropospheric burden of O_3 by $\sim 10\%$. For HNO_3 , there are corresponding increases of upto $\sim 100\%$. Comparing Figs 1 and 3 shows that the largest increases in $[\text{HNO}_3]$ generally occur above the altitude at which the ice particle field exhibits its significant coverage.

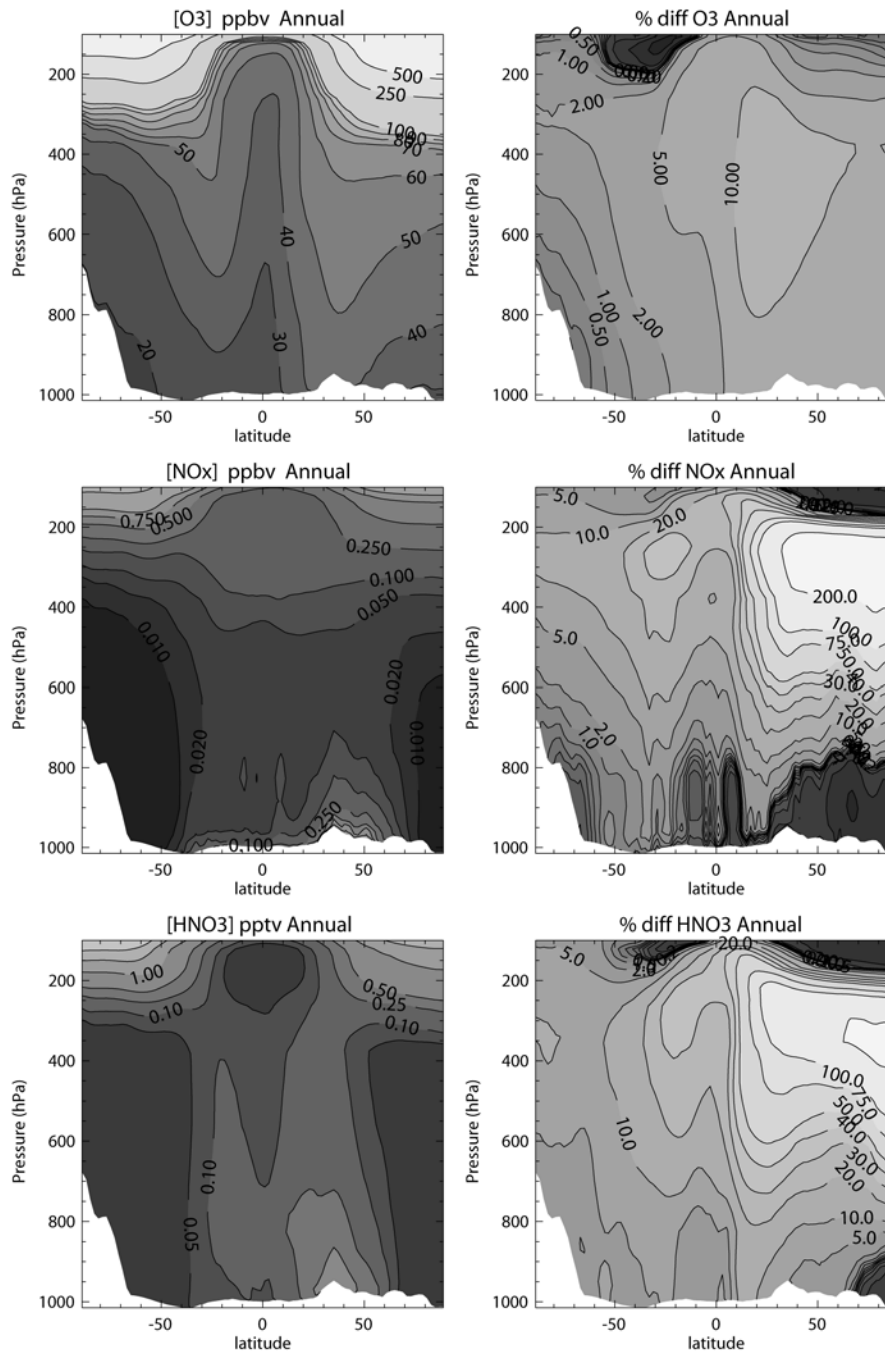


Figure 3: The zonally integrated annual means of (a) O_3 , (b) NO_x and (c) HNO_3 in the BASE simulation and the resulting differences as compared to the BASE_2050 simulation using 2006 meteorology.

3.4 The importance of heterogeneous scavenging with increased aircraft emissions

For the 2050_HNO₃_UP simulation the perturbation in the *in-situ* production of ozone becomes

less important. Table 1 provides the global tropospheric burdens for O₃, CO and HNO₃ for all of the simulations presented. Comparing the values for the BASE and 2050 simulations, it can be seen that the increase in [O₃] substantially reduces the tropospheric burden of CO (although the corresponding future increase in CO emissions are not included in the simulation). For the solid [HNO₃] the total integrated N scavenged onto ice surfaces increases +7% from 0.96 Tg yr⁻¹ (present) to 1.03 Tg yr⁻¹ (future). The percentage increase is less than that which occurs in the gas phase due to both saturation of the available ice surfaces and the differences in altitude between the SAD available and that where the largest increases in HNO₃ occur. The net effect on tropospheric O₃ is to reduce the observed increase which occurs in the present day scenario. In reality the changing climate could also impose an effect by modifying the SAD which is available, where increasing temperatures as a result of an increase in the radiative forcing from (e.g.) O₃ and a positive feedback due to enhanced evaporation (Dressler et al, 2008) would result in a decrease in the incidence of cirrus, thus diminishing the importance of such heterogeneous processes.

Table 1: The changes in the tropospheric burdens of O₃, CO and HNO₃ due to heterogeneous scavenging of HNO₃ onto cirrus particles. All numbers are globally integrated values for the year 2006, where the HNO₃_UP and 2050_HNO₃_UP values are given in paranthesis.

Trace Species	Present Tropo. Burden (Tg)	Future Tropo. Burden (Tg)
O ₃	263.5 (275.5)	295.6 (294.6)
CO	305.7 (292.9)	274.3 (278.5)
HNO ₃	0.645 (0.641)	0.649 (0.645)

4 CONCLUSIONS

In this study we have show that by incorporating simple parameterizations for calculating the micro-physical properties of cirrus particles in a global CTM, we can introduce seasonal and spatial variability in the ice particle fields as constrained by the meteorological input data available in the model. By introducing reversible scavenging of HNO₃ onto ice surfaces we have found that stark differences occur between the Northern and Southern Hemispheres with respect to the perturbation introduced to the in-situ formation of tropospheric O₃. This effect is more modest than that found in previous studies, in that our study gives an increase in the tropospheric O₃ burden as a result of an increase in the availability of reactive nitrogen. The limited amount of scavenging of HNO₃ out of the gas phase means that the effect of de-nitrification due to the gravitational settling of large particles can be neglected. For a more accurate assessment of the global effects, the fraction of HNO₃ lost irreversibly into ice particles needs to be included, along with sub-grid parameterizations to describe the high SAD of contrail cirrus. This should amplify the effects presented here leading the a net global decrease in tropospheric O₃. When adopting future aircraft emission estimates using fixed meteorology for 2006, we find that the fraction of HNO₃ scavenged out of the gas phase is reduced due to saturation effects on the ice surface. Therefore, without a corresponding increase in SAD due to climate changes, which is not likely considering that temperature is likely to increase, the influence of heterogeneous scavenging will become less important.

REFERENCES

- Boersma K. F., D. J. Jacob, H. J. Eskes, R. W. Pinder, J. Wang and R. J. van der A, 2008: Intercomparison of SCIAMACHY and OMI tropospheric NO₂ columns: Observing the diurnal evolution of chemistry and emissions from space, *J. Geophys. Res.*, 113, D16S26, doi:10.1029/2007JD008816.
- Cox, R. A., M. A. Fernandez, A. Symington, M Ullerstam and J. P. D. Abbatt, 2005: A kinetic model for up-take of HNO₃ and HCl on ice in a coated wall flow system, *Phys. Chem. Chem. Phys.*, 7, 3434-3442.
- Dressler, A. E., Z. Zhang and P. Yang, 2008: Water-vapor climate feedback inferred from climate fluctuations, 2003-2008, *Geophys. Res. Letts.*, 35, doi: 10.1029/2008GL035333.
- Grewe, V., M. Dameris, C. Fichter, and R. Sausen, 2002: Impact of aircraft NO_x emissions. Part 1: Interactively coupled climate-chemistry simulations and sensitivities to climate-chemistry feedback, lightning and model resolution, *Meteorologische Zeitschrift*, 11(3), 139ff.
- Heymsfield, A. J. and G. M. McFarquhar, 1996: High albedos of cirrus in the tropical pacific warm pool:

- Microphysical interpretations from CEPEX and from Kwajalein, Marshall Islands, *J. Atmos. Sci.*, 53, 2424-2451.
- Heymsfield, A. J., 2003: Properties of Tropical and Midlatitude Ice Cloud Particle Ensembles. Part II: Applications for Mesoscale and Climate Models, *J. Atmos. Sci.*, 60, 2592-2611.
- Kärcher, B., Abbatt, J. P. D., Cox, R. A., Popp, P. J. and Voigt, C., 2009: Trapping of trace gases by growing ice surfaces including surface-saturated adsorption, *J. Geophys. Res.*, 114, D11306, doi: 10.1029/2009JD011857.
- Labonne, M., F-M Breon and F. Chevallier, 2007: Injection height of biomass burning aerosols as seen from a spaceborne lidar, *Geophys. Res. Letts.*, 34, doi: 10.1029/2007GL029311.
- Lawrence, M. G., and P. J. Crutzen, 1998: The impact of cloud particle gravitational settling on soluble trace gas distributions, *Tellus*, 50B, 263-289.
- Popp, P.J., Gao, R.S., Marcy, T.P., Fahey, D.W., Hudson, P.K., Thompson, T.L., Kärcher, B., Ridley, B.A., Weinheimer, A.J., Knapp, D.J., Montzka, D.D., Baumgardner, D., Garrett, T.J., Weinstock, E.M., Smith, J.B., Sayres, D.S., Pittmann, J. V., Dhaniyala, S., Bui, T.P., and Mahoney, M., 2004 :Nitric Acid Uptake on Subtropical Cirrus Cloud Particles, *J. Geophys. Res.*, 109, D06, doi: 10.1029/2003JD004255.
- Roberts, G., M. J. Wooster, and E. Lagoudakis, 2009: Annual and diurnal biomass burning temporal dynamics, *Biogeosciences*, 6, 849-866.
- Von Kulmann, R., and M. G. Lawrence, 2006: The impact of ice uptake of nitric acid on atmospheric chemistry, *Atms. Chem. Phys.*, 6, 225-235.
- Williams, J. E., and T. P. C. van Noije, 2008: On the upgrading of the modified Carbon Bond Mechanism IV for use in global Chemistry transport Models, KNMI Scientific report WR 2008-02, pp 64.
- Williams, J. E., M. P. Scheele, P. F. J. van Velthoven, J-P. Cammas, V. Thouret, C. Galy-Lacaux and A. Volz-Thomas, 2009: The influence of biogenic emissions from Africa on tropical tropospheric ozone during 2006: a global modelling study, *Atms. Chem. Phys.*, 9, 5729-5749.
- Van der Werf, G. R., Randerson, J. T., Giglio, L., Collatz, G. J., Kasibhatla, P. S., and Arellano Jnr, A. F., 2006: Interannual variability in global biomass burning emissions from 1997 to 2004, *Atms. Chem. Phys.*, 6, 3423-3441.